23rd Australasian Fluid Mechanics Conference - 23AFMC
Sydney, Australia
4 – 8 December 2022

Paper No: AFMC2022-273

Microbubble Generation via Combined Saffman-Taylor and Plateau-Rayleigh Instabilities

Sienna Cook[1], Luka Barbaca[1*], Patrick S. Russell[1], James A. Venning[1], Bryce W. Pearce[1] and Paul A. Brandner[1]

[1] Cavitation Research Laboratory, Australian Maritime College, University of Tasmania, Launceston, TAS 7250, Australia
*mailto: Luka.Barbaca@utas.edu.au

Abstract

Microbubble generation via rapid depressurization of supersaturated water through a 8 mm wide by 2 mm long by 0.1 mm deep Hele-Shaw passage was explored experimentally using micro shadowgraphy. The flow topology consists of a series of regularly sized cellular cavities, characteristic of viscous fingering in a Hele-Shaw flow. Cells develop in a region of separated flow at the sharp leading edge of the confined flow. Each cell is stable and pinned to the wall. Small-scale structures stretch into ligaments downstream and destabilise due to Plateau-Rayleigh instability, with consequent microbubble pinch-off providing a coherent bubble stream from each cell. The influence of cavitation number (σ_{inj}) and Reynolds number (Re) on instability formation and microbubble production is investigated by varying the differential pressure between the passage inlet and outlet. Optimum conditions for bubble generation were found for $\sigma_{inj} = 0.28 - 0.65$ and coincide with the maximum in the number of cells forming along the passage leading edge. Polydisperse bubble populations were generated for all conditions. Bubble production rates of up to 2.2 MHz were observed, with a dominant bubble size of $\approx$ 6μm. Further decrease in σ_{inj} hindered bubble generation due to disappearance of the laminar instability as the flow in the passage transitions to a turbulent regime.

1 Introduction

Within practical engineering situations nucleation is invariably heterogeneous. For cavitation to occur in this case, the water must contain sites of weakness, referred to as ‘nuclei’. Natural nuclei in the ocean and other environments are mainly found in the form of microbubbles, with their population influenced by sea state and water depth. Microbubbles have a critical pressure at which their equilibrium becomes unstable, undergoing explosive growth and subsequent collapse recognised as macroscopic cavitation. The critical pressure of a microbubble is size-dependant and can be lower than the surrounding water vapour pressure, requiring the liquid to be in tension for cavitation inception to occur.

As nuclei may have an influence on a variety of physical processes their dynamics is of interest in broad range of science and engineering applications. Some fields with strong interest in nuclei are naval hydrodynamics, oceanography, sonochemistry, microfluidics, medical drug delivery and non-invasive diagnostics and surgery. Studies in hydrodynamic facilities, such as the Australian Maritime College (AMC) Cavitation Research Laboratory (CRL) have shown that the nuclei population significantly influences cavitation inception and the dynamics of developed cavitation (Brandner *et al.*, 2018, Khoo *et al.*, 2021). In order to accurately model cavitation phenomena, strict control of the nuclei population, i.e. concentration and size distribution of nuclei, is required.

Populations of microbubbles can be classified as monodisperse, where all the bubbles are of the same size, or polydisperse, where the bubbles have various sizes. To be suitable for use as nuclei, bubbles have to be in the size range of $1 - 100$ μm, hence generation and measurement techniques

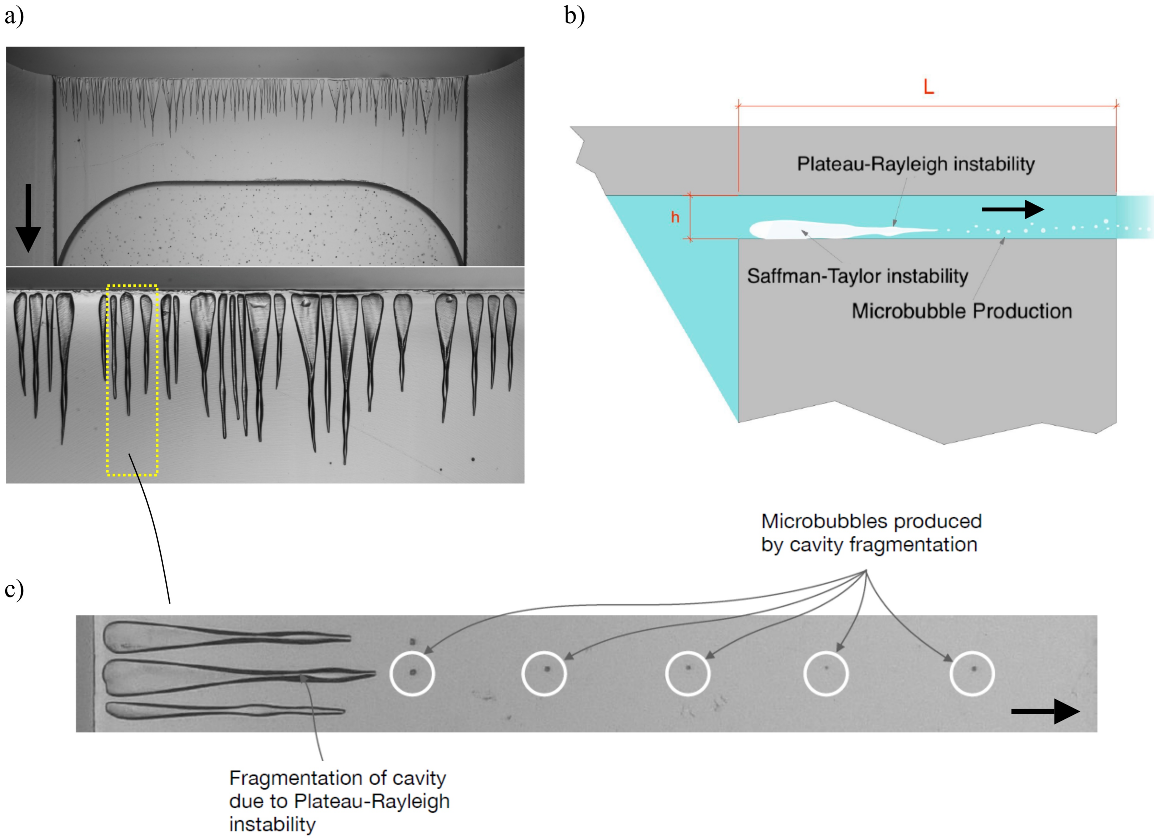

Figure 1. a) Combined instabilities producing quasi-regular cavities that populate the leading edge of a Hele-Shaw device. b) Basic representation of Hele-Shaw flow containing combined instability. Dimensions are $h = 0.1$ mm and $L = 2$mm. c) Typical cellular cavities producing microbubbles via Plateau-Rayleigh instability.

required for experimental modelling of cavitation nucleation at this scale are required.

A common method for microbubble generation is via use of microfluidic devices with operating modes such as: co-flow, cross-flow and flow-focussing, which despite similarities, are based upon independent fluid dynamics phenomena (Rodriguez-Rodriguez *et al.*, 2015). The two techniques currently used at CRL are based on the use of microfluidic T-junctions (Russell *et al.*, 2020), creating monodisperse populations via cross-flow, and devices called mini-tubes, where bubbles are produced via rapid depressurization of supersaturated water through an orifice (Barbaca *et al.*, 2020). However, these techniques do not cover the entire range of microbubble sizes and concentrations and there remains a wider technological demand for further studies to guide design of novel flow configurations to generate microbubbles.

The aim of current work is to explore a new microfluidic device combining two fluid dynamic instabilities, namely, Saffman-Taylor and Plateau-Rayleigh, in a confined flow within a rectangular Hele-Shaw passage (figure 1). In the CRL, exploratory experiments observing pinned cellular cavities in laminar flows of supersaturated water through an 8 mm wide by 0.1 mm thick Hele-Shaw passage have been shown to produce microbubbles.

Images of cavitation in the Hele-Shaw passage show formation of cells along the leading edge due to the Saffman-Taylor instability, with downstream ligament formation. The ligaments destabilise due to the Plateau-Rayleigh instability, with subsequent microbubble pinch-off providing a coherent bubble stream from each cell (figure 1). Observations of this process are not dissimilar to fluid thread break-up, resembling a falling stream of water breaking into smaller packets interpreted as a Plateau-Rayleigh instability. As addressed by Villermaux (2007), there is no reason to think that the same phenomenon of drops produced by a liquid ligament in a gas would not apply to the opposite situation of bubbles produced by a gas ligament in a continuous liquid phase.

2 Methodology

The experiments were performed at the AMC CRL. The base of the experimental apparatus is a custom designed Hele-Shaw device supplied with supersaturated water. The water is saturated, pressurised and supplied to the device via a separate pressure plenum at pressures in the range 150-1000 kPa. The pressure plenum also acts as a water reservoir. The saturation vessel pressure is measured using a Wika gauge pressure transducer Model P-10 with a precision of 0.1%. Atmospheric pressure is measured using a Vaisala Model PTB210 digital barometer with a precision of $\pm$0.03 kPa. The volumetric flow rate of supersaturated water supply to the microbubble generator is calculated based on the time rate of change of water level in an isolated calibrated pipe chamber using an Orion Instruments magnetically coupled liquid level sensor with a precision of $\pm$0.5%. The Hele-Shaw device is made of transparent acrylic and manufactured using conventional machining techniques. The internal dimensions of Hele-Shaw passage are 8 mm wide by 2 mm long and 0.1 mm deep.

Observations of cells and microbubbles were obtained using micro shadowgraphy setup consisting of a Nikon D850 DSLR camera (resolution 8256 $\times$ 5504 pixels), equipped with a Laowa 25 mm 2.5-5X Ultra Macro lens. Back illumination was provide by a xenon strobe (Sugawara Lamphouse NPL-180/Nano Light Strobedriver NP-3A) with 180 ns pulse duration. For the analysis of the topology of cellular structures, the images were acquired at 2.5X magnification, with a resulting field-of-view of 14 $\times$ 9.4 mm and spatial resolution of 1.7 µm/pixel. Microbubble production was analysed using images acquired at 5X magnification, with corresponding field-of-view of 7.4 $\times$ 5 mm and a spatial resolution of 0.9 µm/pixel. A schematic of the experimental setup is presented in figure 2.

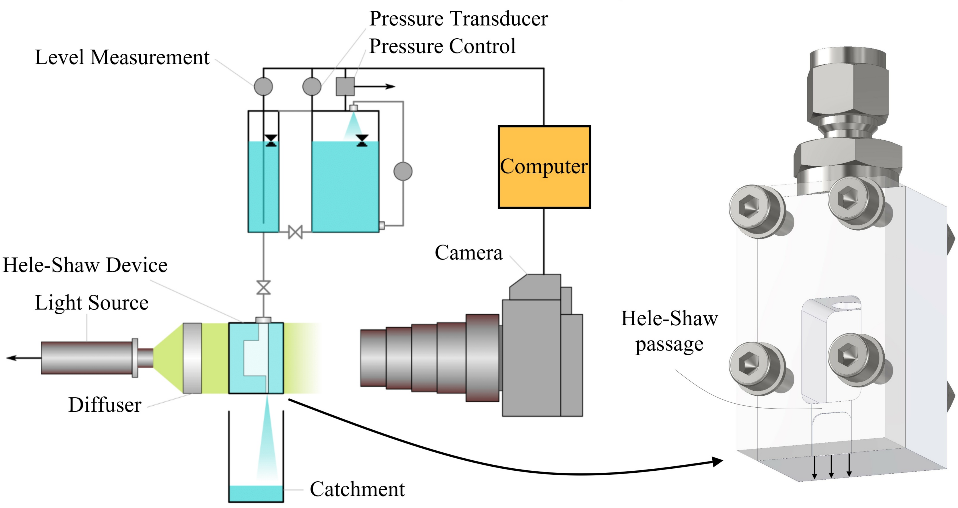

Figure 2. A schematic of the experimental apparatus used for microbubble generation and imaging.

Two main parameters controlling the flow topology and resulting microbubble production in the Hele-Shaw passage are cavitation number:

$$\sigma_{inj} = \frac{p_{down} - p_v}{P_{up} - p_{down}} \tag{1}$$

and Reynolds number calculated as:

$$Re = \frac{U_{jet} h}{\nu} \tag{2}$$

In this work, σ_{inj} and Re were controlled by varying the supply pressure p_{up}, while Hele-Shaw passage outlet was open to the atmosphere. As both, σ and Re, are controlled by variation in differential pressure between the device inlet and outlet, the effect of these parameters could not be investigated independently. Pressure downstream of the confined flow, p_{down}, is taken as atmospheric pressure, p_v is vapour pressure, h is the depth of the Hele-Shaw passage and ν is the water kinematic viscosity. U_{jet} is calculated as the nominal velocity through the Hele-Shaw passage as:

$$U_{jet} = \sqrt{\frac{2(p_{up} - p_{down})}{\rho}} \tag{3}$$

where ρ is the water density. The dimensionless discharge coefficient, C_d, can be defined as:

$$C_d = \frac{U}{U_{jet}} \tag{4}$$

where U is the measured average velocity in the Hele-Shaw passage, calculated from the flow rate Q and the Hele-Shaw passage cross-sectional area. Across the range of investigated p_{up} values, σ_{inj} varied between 0.11 and 1.94 and Re between 341 and 2,250.

Cell width data were acquired for a pressure range 150-1000 kPa in increments of 50 kPa, with more detailed measurements acquired in 25 kPa increments for the pressures in range 200-400 kPa. For each condition, 30 images of the flow in Hele-Shaw passage were taken. Cell widths were measured using a pixel ruler from selected images and converted into length scale using the calculated spatial resolution.

Optimum conditions for microbubble generation were determined to be in the range 250 kPa $\leq p_{up} \leq$ 450 kPa. Microbubble populations were measured in this range in 50 kPa increment. For each condition 210 images were acquired. In order to detect, locate and size the bubbles, images were processed using LaVision DaVis software with the Particle Master module.

3 Results

The general structure of cavitation in a Hele-Shaw passage, reflects the combined Saffman-Taylor and Plateau-Rayleigh instability. The cavitation topology consists of a series of regularly sized cellular cavities, characteristic of viscous fingering in Hele-Shaw flow, detaching from the separation at the sharp leading edge of the confined flow. Each small cavity is stable and pinned to the wall, with gas diffusion into the cell balancing mass flux due to bubble pinch-off. These small-scale structures stretch into ligaments downstream and destabilise due to Plateau-Rayleigh instability, with subsequent microbubble pinch-off providing a coherent bubble stream from each cell (figure 1). As σ_{inj} decreases and Re increases, cells amalgamate into large, disparate cavities typical of boundary layer separation (figure 3). As σ_{inj} and Re were not controlled independently in this preliminary study, it was not possible to determine the independent effect that these parameters have on cell formation and behaviour.

For $\sigma_{inj} \leq 0.24$, a coalescing bubble cloud in the shear layer downstream of Hele-Shaw passage is visible, drawn together by the formation of larger cavities and becoming increasingly coherent (figure 3). The turbulent transition is evident in the vortical recirculation of water. Note for $\sigma_{inj} = 0.65, 0.32, 0.15$ and $0.12 - 0.11$ the confined flow detached from the Hele-Shaw downstream edge as a jet leading to a different appearance. For $\sigma_{inj} \leq 0.14$ kPa cavities extend along the complete length of the Hele-Shaw passage. For these high Re cases, it is apparent that the cells must have an effect on the behaviour of the flow downstream, as constant laminar streamlines directly downstream of the cells can be seen through an otherwise turbulent flow. This flow regime is similar to the behaviour of liquid jets through nozzle orifices at reduced cavitation numbers, often labelled as 'hydraulic flip' (Stanley, 2012).

Dependence of the discharge coefficient, C_d, on σ_{inj} and Re is presented in figures 4a and 4b, respectively. Low C_d (0.3 - 0.5) values are expected as the flow resistance and irrecoverable losses in

Figure 3. Sample photographs of cavitation topology in the Hele-Shaw cell across the range of investigated inlet pressures. The respective cavitation number values are indicted in each image. Note the visible transition of the flow downstram of the Hele-Shaw from laminar to turbulent with an increase in inlet pressure.

a Hele-Shaw passage are much greater than the typical nozzle type orifices. This can be attribute to the complex behaviour of the fluids at the microscale, where surface tension and fluid resistance tend to dominate flow characteristics.

Dependence of C_d on σ_{inj} appears to be linear (figure 4a). For low Re values C_d increases sharply, however, for high $Re \geq 1500$, C_d reaches an asymptotic value ($C_d = 0.45 - 0.5$) (figure 4b). This can be related to the flow transition from a laminar to a turbulent regime. Again, this is indicative of the microscale behaviour dominating the properties of the flow, with the upper limit in C_d defined by the geometry of the device and the physical properties of water at this scale.

A quantitative description of the topology of the cellular structures at the Hele-Shaw passage leading edge is presented in figure 5. Cells start to consistently appear for $\sigma_{inj} \leq 1$. A peak in the cell count was observed for $\sigma_{inj} \approx 0.5$, where ≈ 80 cells form along the passage leading edge (figure 5a). With a further decrease in σ_{inj}, the cell number decreases to be below 10 as small semi-regular cavities amalgamate into larger structures. For the conditions where developed cellular structure is present ($\sigma_{inj} = 0.28 - 0.65$), a dominant cell width of about $50 - 60$ µm is observed (figure 5b). The peak becomes less prominent with decrease in σ_{inj}. Overall, the quantitative data presented in figure 5 matches with the qualitative observations from still photography in figure 3.

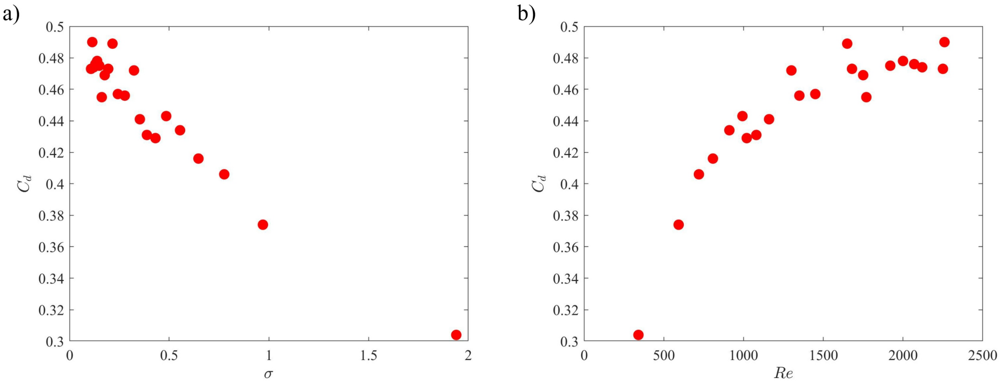

Figure 4. a) C_d as function of σ_{inj}. b) C_d as function of Re. Discharge coefficient reaches an asymptotic value as the flow undergoes transition from laminar to turbulent regime.

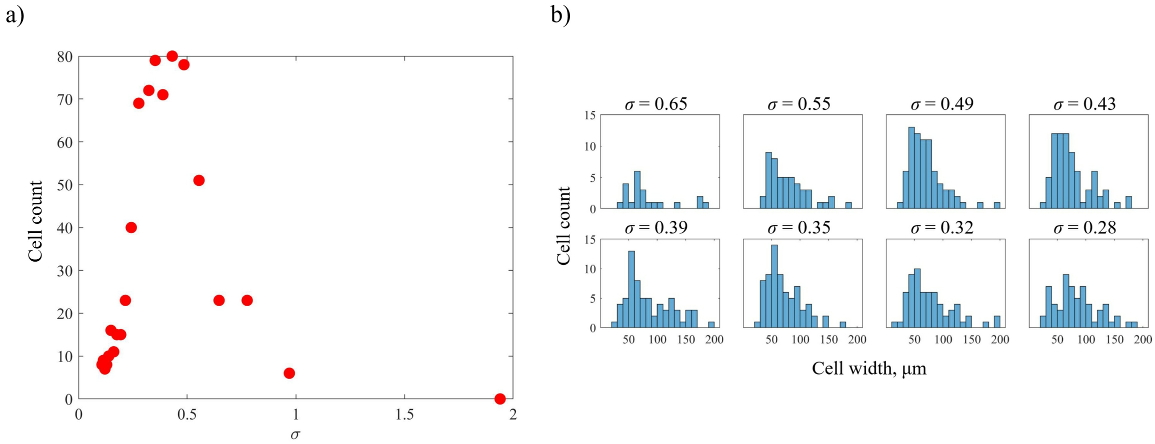

Figure 5. a) Total cell count along the leading edge of the Hele-Shaw device across the range of investigated σ values. The leading edge is only fully populated with uniformly sized cells within a relatively narrow range of $\sigma_{inj} = 0.28 - 0.49$. For $\sigma_{inj} \leq 0.28$, cells amalgamate into larger cavities, decreasing the total population along the leading edge. b) Histograms of cell widths for $\sigma_{inj} = 0.28 - 0.65$. A dominant cell size of about $50 - 60$ µm is observed for all pressures. Histograms are presented with 10 µm bin size.

Bubble size distributions for the microbubble populations generated for $0.28 \leq \sigma_{inj} \leq 0.65$ are presented in figure 6 as histograms with a 2 µm bin size. For all the populations, a peak in bubble count is observed as the bubble diameter approaches the lower resolution limit of the optical system used (≈ 6 µm). A power law like decay with increase in bubble size is observed in all cases. Overall, the majority of generated bubbles appear to be very small, with a negligible number of bubbles larger than 30 µm produced. With a decrease in σ_{inj} an increase in bubble production is observed across all bins. This is further evident in figure 7, where the dependence of the total bubble production rate, f_{tot} on σ_{inj} is presented. The device is shown to produce a large quantity of bubbles in all instances where cellular structure is observed ($O \sim$ MHz), with an increase of about an order of magnitude observed between the extremes of the investigated σ_{inj} values.

Enlarged images of the passage leading edge (figure 8) revealed that the otherwise smooth edge is rugged at the microscale. Along the leading edge, the vast majority of cells appear attached directly downstream of visible concavities. The cells form repeatedly along the particular sections of the leading edge, yet the size of those cells is not always consistent, determining where and how the cell either side forms.

It is also evident that some sections of the leading edge, often with deeper defects, are consistently empty of the cells; implying that cell formation is dependant on the grade of the edge roughness. This is consistent with the attempts to manufacture identical Hele-Shaw devices with conventional

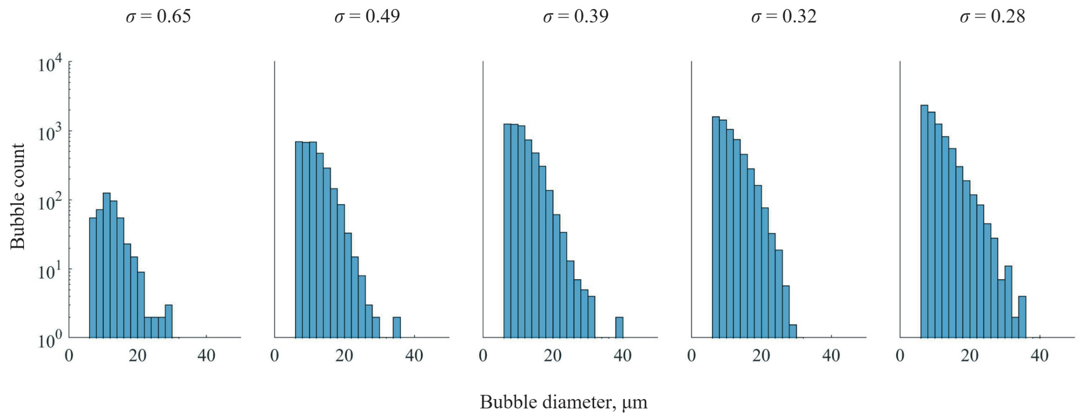

Figure 6. Histograms of microbubble diameter produced by cavitation in Hele-Shaw device. For all pressure a peak in bubble production is observed near the lower resolution of the used optical system. Histograms are presented with a 1 μm bin width.

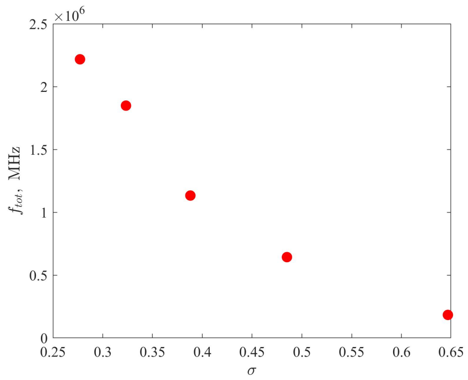

Figure 7. Microbubble production rate as a function of σ_{inj} for range $0.28 \leq \sigma_{inj} \leq 0.65$.

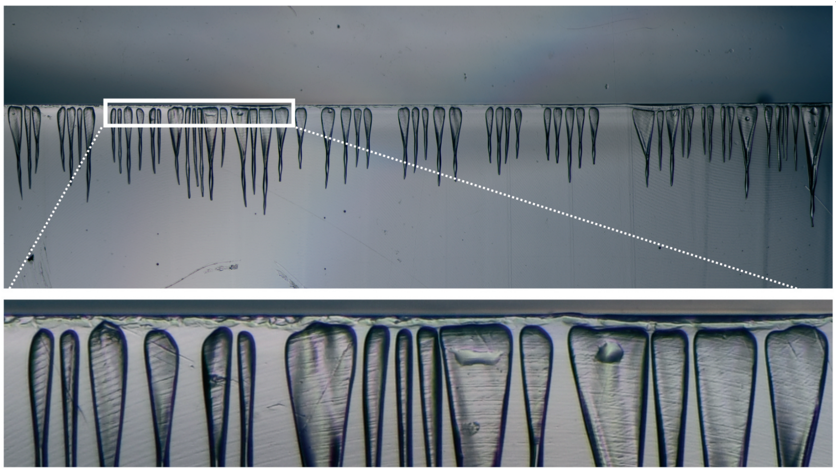

Figure 8. Still photographs examing perturabation along the leading edge of Hele-Shaw passage ($\sigma_{inj} = 0.49$). Edge defects along the leading edge perturb the flow and allow the formation of cell cavities. Small irregularities along the edge appear to generate smaller, more uniform, cells.

machining, which did not always yield a similarly consistent, large populations of cavities across the entire width of the passage leading edge.

4 Conclusions

Cellular cavities at the leading edge of a Hele-Shaw passage were shown to generate microbubbles through a process attributed to combined Saffman-Taylor and Plateau-Rayleigh instabilities. Optimum mirobubble generation conditions were found to coincide with the maximum in the number of cells forming along the leading edge for $\sigma = 0.28 - 0.68$. For these conditions, the device generates a polydisperse microbubble population at the rates of up to 2.2 MHz, with a dominant size close to the lower resolution limit of the optical system used (≈ 6 μm). Further decrease in cavitation number resulted in a decrease in bubble production rate due to the transition of the flow from a laminar to turbulent regime, preventing cavity formation.

The formation and topology of the leading edge cavities were found to be affected by flow perturbations induced by surface irregularities at the Hele-Shaw passage leading edge. Further work is required to establish the exact mechanisms involved with this phenomena. A study of a device with homogeneously distributed surface irregularities micro-machined into the passage leading edge is planned for the future.

Acknowledgements

The authors wish to acknowledge the assistance of Mr Robert Wrigley and Mr Steven Kent in carrying out the experiments. The authors wish to acknowledge the support of Australian Defence Science and Technology Group within the framework of the University of Tasmania collaborative work on Office of Naval Research 2017 US Multidisciplinary University Research Initiative (MURI) titled ‘Predicting turbulent multi-phase flows with high-fidelity: a physics-based approach’.

References

Barbaca, L., Russell, P.S., Pearce, B.W. and Brandner, P.A. 2020, Characterization of microbubble generation in a confined turbulent jet, *Proceedings of the 22nd Australasian Fluid Mechanics Conference*

Brandner, P.A. 2018, Microbubbles and cavitation: Microscales to Macroscales, *Proceedings of the 10th International Symposium on Cavitation - CAV2018*

Khoo, M.T., Venning, J.A., Pearce, B.W. and Brandner, P.A. 2021, Nucleation and cavitation number effects on tip vortex cavitation dynamics and noise, *Experiments in Fluids*, 62(10):216

Rodriguez-Rodriguez, J., Sevilla, A., Martinez-Bazan, C. and Gordillo, J.M. 2015, Generation of microbubbles with applications to industry and medicine, *Annual Review of Fluid Mechanics*, 47(1)

Russell, P.S., Venning, J.A., Pearce, B.W. and Brandner, P.A. 2020, Calibration of Mie Scattering Imaging for microbubble measurement in hydrodynamic test facilities, *Experiments in Fluids*, 61(4)

Stanley, C., 2012, Experimental investigation of cavitation in cylindrical orifice, *School of Mechanical and Manufacturing Engineering, University of New South Wales*

Villermaux, E., 2007, Fragmentation, *Annual Review of Fluid Mechanics*, 39(1)